An Excitonic Pentamer Model for the Core Q_y States of the Isolated Photosystem II Reaction Center

R. Jankowiak,* J. M. Hayes, and G. J. Small*

Ames Laboratory—USDOE and Department of Chemistry, Iowa State University, Ames, Iowa 50011

Received: January 10, 2002; In Final Form: April 11, 2002

An excitonic pentamer model (an adaptation of the multimer model; Durrant et al. *Proc. Natl. Acad. Sci. U.S.A.* **1995**, *92*, 4798) is proposed for the core Q_y states of the photosystem II reaction center (PSII RC). The core chlorins consist of four chlorophyll *a* molecules (P_1, P_2, Chl_1, Chl_2) and two pheophytin *a* molecules ($Pheo_1$, $Pheo_2$). In the pentamer model $Pheo_2$ on the inactive D_2 branch is, for all intents and purposes, decoupled from the other five chlorins. This model is the result of theoretical simulations of several types of spectra obtained at liquid helium temperatures in the Q_y region and the Pheo Q_x region of the absorption spectrum. They include bleaching spectra obtained by reduction of $Pheo_2$ with dithionite (in the dark) and reduction of the active $Pheo_1$ with dithionite and white light illumination, triplet bottleneck hole spectra, and femtosecond pump−probe spectra (from S. R. Greenfield et al. *J. Phys. Chem. B* **1999**, *103*, 8364). The model structure of Svensson et al. of PSII RC (*Biochemistry* **1996**, *35*, 14486) and the recent X-ray RC structure of Zouni et al. (*Nature* **2001**, *409*, 739) were used to construct hexamer excitonic Hamiltonians. Both Hamiltonians, with uncorrelated site excitation energy disorder taken into account, yield similar results and acceptable fits to the spectra *but* only if $Pheo_2$ is decoupled. Such decoupling would require a significant weakening of the $Pheo_2$–Chl_2 interaction predicted by the RC structures. Possible reasons for weakening are given. Our findings include the following: (1) The localized Q_x/Q_y transitions of $Pheo_2$ are at 541.2 and 668.3 nm with absorption bandwidths of $\sim$200 cm^{-1}. (2) The Q_x transition of $Pheo_1$ is at 544.4 nm with an absorption bandwidth of $\sim$200 cm^{-1}. (3) Within the pentamer model four of the five Q_y states are delocalized over both the D_1 and D_2 branches. The delocalization results in significant narrowing ($\sim$40%) of inhomogeneous spectral broadening that stems from the width of the site (chlorin) excitation energy distribution functions. (4) The contributions of P_1 and P_2 to the lowest energy (primary donor, P680*) state are, on average, the largest although the contributions from the other three chlorins are significant. (5) The triplet state associated with the bottleneck spectrum appears to be localized on Chl_1 (or P_2). (6) The combined absorption dipole strength of $Pheo_1$ associated with the two lowest energy and strongly absorbing states (separated by only $\sim$80 cm^{-1}) is equivalent to that of $\sim$1.8 monomer Pheo molecules. This finding provides a plausible explanation for the results of Greenfield et al. The paper ends with discussion of the nature of P680* and the triplet state(s) formed by charge recombination of the primary radical ion pair.

1. Introduction

In oxygenic organisms, which include higher plants, algae, and cyanobacteria, it is the high oxidizing potential of the oxidized primary electron donor ($P680^{\bullet+}$) of the D_1/D_2-Cyt b_{559} photosystem II (PSII) reaction center (RC) which drives secondary reactions that ultimately lead to splitting of water. Since its isolation in 1987 from spinach,[1] the excited-state electronic structure and excitation energy transfer and charge separation processes of the PSII RC have been subjects of intense study. Biochemical and biophysical studies had indicated early on that[2−8] some of the general features of the PSII RC are homologous to those of the bacterial RC. For example, the D_1 and D_2 polypeptides are structurally analogous to the L and M subunits of the bacterial RC. Until quite recently, the chlorophyll *a* (Chl *a*) content of the PSII RC was controversial, ranging between four and six (and even higher) Chl *a* molecules per two pheophytin *a* (Pheo *a*) molecules.[9] It is now known that the RC contains six Chl *a* molecules and two Pheo *a* molecules, two plastoquinones, a non-heme iron, two β-carotenes, and one or two cytochrome b_{559} (Cyt b_{559}) molecules.[8−10] (In what follows the reaction center containing six Chl *a* molecules will be referred to as RC-6.) The structural arrangement of the four core Chl *a* molecules and two Pheo *a* molecules is shown in Figure 1. $P_{1/2}$, $Chl_{1/2}$, and $Pheo_{1/2}$ are structurally analogous to $P_{L/M}$ (special pair), $BChl_{L/M}$, and $BPheo_{L/M}$ of the bacterial RC.[2] The two Chl *a* molecules not shown are bound to histidines at the peripheries of the D_1 and D_2 polypeptides. They are often referred to as Chl_{Z1} and Chl_{Z2}.[8] The bacterial RC does not possess peripheral BChl molecules. In both RCs a pseudo-C_2 rotation axis relates the two branches, D_1/D_2 and L/M.

The structure shown in Figure 1 is based on the coordinates of the PSII RC structure of Svensson et al.[7] The center to center distance between P_1 and P_2 is 10.1 Å, which is significantly longer (by 2.5 Å) than the distance between P_L and P_M in the *Rhodopseudomonas (Rps.) viridis* RC (other chlorin−chlorin distances are given in the figure caption). Very recently, the X-ray crystal structure of PSII from the cyanobacterium *Synechococcus elongatus* was reported at 3.8 Å resolution.[10] It appears that the structural arrangements of the core chlorins in

* To whom correspondence should be addressed. E-mail: jankowiak@ameslab.gov (R.J.); small@iastate.edu (G.J.S.).

10.1021/jp020050l CCC: $22.00
Published on Web 08/03/2002

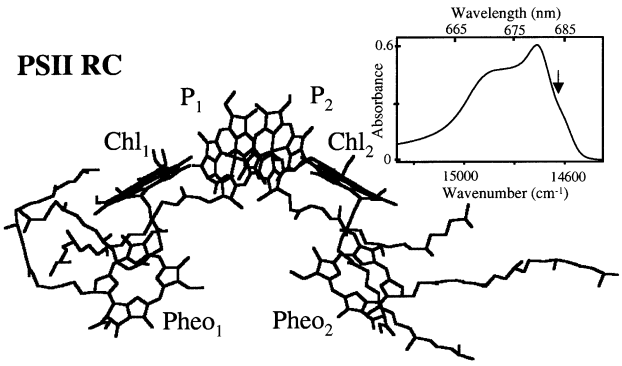

Figure 1. Arrangement of the cofactors in the PSII RC core according to the Svensson et al. RC structure. P_1, Chl_1, and $Pheo_1$ and P_2, Chl_2, and $Pheo_2$ are the pigments that belong to the active and inactive branches, respectively. The center to center distance between the P_1 and P_2 Chl molecules is 10.1 Å, and the distances between P_1 and Chl_1, P_2 and Chl_2, Chl_1 and $Pheo_1$, Chl_2 and $Pheo_2$, and $Pheo_1$ and $Pheo_2$ are 9.9, 9.4, 10.4, 11.5, and 23.1 Å, respectively. The inset shows the Q_y region absorption spectrum of RC-5 at 4.2 K. The origin of the shoulder near 684 nm (arrow) is still a matter of debate (see the text).

the X-ray structure are similar to those in the structure of Svensson et al. In the X-ray structure the center to center distances between the accessory Chl_1/P_1 and Chl_2/P_2 are 9.8 and 10 Å, respectively. In both structures the Chl_1 and Chl_2 planes are tilted by about 30° with respect to the membrane plane, similar to the tilt angle of $BChl_L$ and $BChl_M$ in the bacterial RC. The center to center distances between Chl_1 and $Pheo_1$ and between Chl_2 and $Pheo_2$ are 10.7 and 10.6 Å, respectively. The distance between $Pheo_1$ and $Pheo_2$ is 22.8 Å. All these distances are similar to those in the structure of Svensson et al.; see the Figure 1 caption. Importantly, the $P_{1-}P_2$ distance in the X-ray structure is 10 Å, within experimental uncertainty identical to the value of Svensson et al. The lengthening of the P_1-P_2 distance by 2.5 Å relative to that of P_L-P_M is, perhaps, the most important structural difference between the cofactors of the two RCs from the perspective of excitonic coupling. For *Rps. viridis*, the splitting between the upper (P_+) and lower (P_-) dimer levels of the special pair of BChl *b* molecules is 1900 cm^{-1} in the low-temperature limit,[11−13] corresponding to a P_L-P_M coupling energy of ∼1000 cm^{-1}. The splitting for *Rhodobacter sphaeroides* with its BChl *a* molecules is ∼1300 cm^{-1}.[13,14] As reviewed in ref 13, electronic structure calculations have predicated that about half of the P_L-P_M coupling is due to electron-exchange coupling. Such coupling should be markedly reduced in $P_{1-}P_2$ because of the 10 Å separation distance, and is most likely negligible relative to the electrostatic coupling. That the distances between the cofactors of the PSII RC are about 10 Å is consistent with the weak electron−phonon coupling and small linear pressure shift rates (∼−0.07 cm^{-1}/MPa) observed for spectral holes burned within the main Q_y absorption band at 680 nm.[15] Weak electron−phonon coupling and small pressure shift rates are expected when electron-exchange coupling, which introduces charge-transfer character to the Q_y states, is weak.[16] An early estimate of 140 cm^{-1} for the electrostatic coupling between P_1 and P_2 was reported in ref 17, where a separation distance of 10 Å was used. The calculation assumed that the relative orientation of the P_1 and P_2 transition dipoles is the same as in the bacterial RC. The 4.2 K triplet bottleneck hole spectra in refs 15 and 18 provided some support for a 140 cm^{-1} coupling in that a relatively weak hole was observed at ∼300 cm^{-1} higher energy than the intense P680 hole. At that time the prevailing view was that P680 is mainly contributed to by P_1 and P_2. By analogy with the bacterial RC, it was often assumed that Q_y absorption bands could be assigned to excitations highly localized on $Pheo_1$, $Pheo_2$, Chl_1, and Chl_2 of the core.

That assumption and the assumption that the primary electron donor state P680* (* ≡ excited state) is the lowest excitonic dimer level (P_-) of P_1 and P_2 were called into question by Durrant et al.,[19] who introduced the so-called multimer model (see also refs 20 and 21). Their excitonic calculations for the six core chlorins (Chl_{Z1} and Chl_{Z2} could be excluded given their peripheral locations), which took into account diagonal energy disorder, indicated that the Q_y states are significantly delocalized over about three chlorins, mainly on either the D_1 or D_2 branch. Two strongly absorbing lowest energy transitions in the ∼680−684 nm range were predicted. $Pheo_1$ and $Pheo_2$ were found to contribute significantly to these states. Although extensive delocalization of the Q_y states might seem surprising given that the strongest pairwise Coulombic couplings are only ∼80−140 cm^{-1} (see section 3), it must be kept in mind that the Q_y absorption spectrum spans a range of only ∼500 cm^{-1}, as shown in the inset of Figure 1 for an RC sample in which the Chl_Z molecule that absorbs near 670 nm has been removed. In what follows we refer to such samples as RC-5. About 20% of the 500 cm^{-1} width is due to inhomogeneous broadening. When the differences between the average chlorin transition energies are comparable to the coupling energies, delocalization is to be expected. Durrant et al. assumed that the transition energies of the six core chlorins are equal, 14860 cm^{-1} (673 nm), an assumption we will argue is reasonable. An important prediction of the multimer model is that reduction or oxidation of any cofactor should cause strong bleaching in the 680−684 nm region. The 4.2 K results in ref 22 on bleaching of the Q_y absorption spectrum of RC-5 after reduction of $Pheo_2$ by sodium dithionite in the dark provided no support for $Pheo_2$ being part of the multimer model. That is, no prominent bleach in the 680−684 nm region was observed. A prominent bleach at ∼668 nm with a fwhm of ∼200 cm^{-1} was observed and assigned to a Q_y state localized on $Pheo_2$. Consistent with this assignment was the observation of a bleach of the $Pheo_2$ Q_x band. Merry et al.[21] concluded that at least one pheophytin (presumably $Pheo_1$) must be coupled to the other reaction center chlorins. Guided by earlier works,[23−25] a prominent bleach at 680 nm for RC-5 with a width of ∼120 cm^{-1} produced by dithionite and white light illumination was assigned to a Q_y state localized on $Pheo_1$ that is quasi-degenerate with P680*.[22,26] However, that assignment was based on the assumption that a Q_y state localized on $Pheo_1$ exists as is the case for $BPheo_L$ in the bacterial RC, which, in light of the calculations of Durrant et al., can be questioned. It might also be questioned because the Q_y band of Pheo *a* in solution lies at ∼665 nm.[9] In methanol solution at apparent pH values of 7 and 2 it is located near 665 and 654, respectively (unpublished results). That is, it is unclear whether interactions of $Pheo_1$ with its protein environment could lead to a red shift to 680 nm. The results presented here indicate that a localized $Pheo_1$ state is very unlikely.

Some support for the prediction of the multimer model that $Pheo_1$ and $Pheo_2$ are involved in excitonic delocalization came from room-temperature femtosecond pump−probe experiments which showed that[27] excitation at 694 nm results in a large (∼40%) prompt (within 300 fs) bleaching of the Pheo Q_x band at 545 nm. This band is not resolved into $Pheo_1$ and $Pheo_2$ components at room temperature. The observation that reduction of the $Pheo_1$ at room temperature results in a significant decrease in the circular dichroism (Q_y) of RC-6 provided some additional support for its involvement in delocalization.[23] The 4.2 K results reported in ref 22 for RC-5 led to the conclusion that the $Pheo_1$

and $Pheo_2$ components lie at 544.4 and 541.2 nm, respectively, with absorption widths of ~200 cm^{-1}, $Pheo_1$ being the Pheo active in primary charge separation. The low-temperature results of ref 28 also placed the $Pheo_1$ Q_x band at ~545 nm, on the low-energy side of the Q_x band. The ability to spectroscopically distinguish between the two Q_x bands in pump−probe experiments is essential for determining whether the D_1 branch is indeed the only one active in charge separation, as is the case for the L branch of the bacterial RC. Resolution at low temperatures of the Q_x bands of $BPheo_L$ and $BPheo_M$ in the static absorption spectra of the wild type and mutants of the bacterial RC was critical in establishing the one-sided electron transfer in bacterial RCs.[29] It has only been recently that mutants have been constructed which exhibit electron transfer down the M branch.[30]

This paper is organized as follows: Materials and experimental methods and computational methods are described in sections 2 and 3, respectively. Section 4.A describes dark reduction experiments with dithionite. In section 4.B we present experimental results on RC-5 obtained at 4.2 K and an analysis of the recent femtosecond pump−probe spectra (7 K) of Greenfield et al.[31] on RC-6, which, together with the results of the excitonic calculations for the Q_y states, provide further support for the $Pheo_1$ and $Pheo_2$ Q_x bands lying on the low and high sides of the unresolved Pheo Q_x band at ~543 nm. Furthermore, the results indicate that the $Pheo_2$ Q_y state, unlike the $Pheo_1$ Q_y state, is decoupled from those of the other cofactors. As a result, we introduce a pentamer model for the core Q_y states of the PSII RC (the two peripheral Chl_Z molecules being excluded). It is emphasized that the low-temperature results of Greenfield et al. point to $Pheo_1$ contributing significantly to the two lowest energy Q_y states that absorb near 680 nm. Further support for this comes from the experimental results and results from excitonic calculations on the Q_y states presented in section 4.C. The latter allow for a detailed analysis of the chlorins that contribute to P680* (* ≡ Q_y state), the lowest energy and primary electron donor state. It is found that, on average, the contributions from P_1 and P_2 are greatest although the contributions from $Pheo_1$ and Chl_1 are significant. Delocalization of the Q_y states was found not to be mainly restricted to either the D_1 and D_2 branches, contrary to the conclusion reached by Marry et al.[21] based on the excitonic Hamiltonian derived for the PSII RC model based on the *Rps. viridis* structure.[19] The experimental results and calculated triplet bottleneck hole spectra indicate that the triplet state is localized on Chl_1, in agreement with the absorption-detected magnetic resonance (ADMR) experiments of van der Vos et al.[32] and Rutherford et al.[33] The pentamer model predicts that the active $Pheo_1$ can be transiently decoupled from the other chlorins by formation of $^3Chl_1$ and that the Q_y band of the decoupled $Pheo_1$ lies at ~673 nm with a width of ~180 cm^{-1}.

2. Materials and Experimental Methods

PSII RC-5 samples were prepared according to Vacha et al.[35] from PSII-enriched membrane fragments obtained from market spinach as described in ref 36. Pigment content analysis was performed on 80% aqueous acetonic extract using the spectrophotometric method of Eijckelhoff and Dekker.[37] The samples contained 5.2 ± 0.3 chlorophylls per two pheophytins, similar to that reported in ref 22. For further details see refs 22 and 34. For low-temperature studies, glycerol was added to the samples (66% v/v) to ensure glass formation with high optical quality. The samples contained ~1 mM dodecyl maltoside (pH 6.5) and were stored at −80 °C until use.

Protein mass from the RC-5 preparation was extracted according to ref 37 and reconstituted with Cyt b_{559} in buffer solution. The absorption spectra (4.2 K) showed no evidence of residual chlorins. Cyt b_{559} was reduced by dithionite (4 mg/mL) in a helium atmosphere at $T \approx 4$ °C and under dim light. The same conditions were used to reduce $Pheo_2$ in RC-5 under dim light to avoid reduction of $Pheo_1$. The active $Pheo_1$ was selectively reduced at 4.2 K by white light illumination in the presence of dithionite.[22−25] A 50 W tungsten−halogen lamp was used as the light source. A 10 cm water cell was placed between the lamp and cryostat to minimize sample heating. The illumination time was 40 min. The dark and white light reduction experiments of Pheo *a* in RC-5 were repeated several times. The results were reproducible if the samples were handled under very dim light in a helium atmosphere at $T \approx 4$ °C. Absorption and triplet bottleneck hole spectra were recorded with a Bruker HR120 Fourier transform spectrometer operated at 4 cm^{-1} resolution. A Coherent CR699-21 CW ring dye laser (line width of 0.07 cm^{-1}) pumped by a 6 W Coherent Innova argon ion laser was used for hole burning. The triplet bottleneck hole-burned spectra correspond to the difference between absorption spectra obtained with the laser on and off. An excitation wavelength of 665 nm and a burn intensity of 75 mW/cm^2 were used. Samples were cooled to 4.2 K using a Janis 8-DT Super Vari-Temp liquid helium optical cryostat. The temperature was stabilized and measured with a Lakeshore Cryotronic model 330 temperature controller.

3. Theoretical Methods and Q_y Excitonic Hamiltonians

Excitonic calculations for the Q_y states were performed using the Frenkel Hamiltonian (static lattice approximation)

$$H = \sum_n (\epsilon_n + d_n)|n\rangle\langle n| + \sum_{n,m}{}' V_{nm}|n\rangle\langle m| \qquad (1)$$

where $|n\rangle$ denotes the localized Q_y state of chlorin *n*. As in ref 19, the peripheral Chl *a* molecules were excluded because of the large distances between them and the core cofactors. ϵ_n is the average monomer transition energy, and d_n is the offset energy due to diagonal site excitation energy disorder that stems from the intrinsic structural disorder of proteins. Guided by low-temperature spectra[22] (see also section 4.B), the site excitation energy distribution function (SDF) for each cofactor was assigned a width of 210 cm^{-1} and described by a Gaussian, the same as that used by Durrant et al.[19] Given this sizable width and that the Q_y absorption spectrum spans a range of only ~500 cm^{-1}, ϵ_n was set equal to 14860 cm^{-1} (673 nm) for all cofactors, as in refs 19 and 20. Justification for the assumption of equal ϵ_n values is given in section 4.C. Excitonic couplings, V_{mn}, were calculated in the point transition dipole−dipole approximation. Dipole strengths of 23 and 14 D^2 for the Q_y states of Chl *a* and Pheo *a* were used.[38] Two model structures were employed. For both the Q_y transition dipoles of the six core chlorins were taken to be parallel to the line between the nitrogens of rings I and III, as is routinely done. Model I is based on coordinates from the PSII RC structure of Svensson et al.[38] (Brookhaven Protein Data Bank file 1DOP). Model II is based on the X-ray coordinates of the PSII RC structure recently obtained by Zouni et al.[10] (Brookhaven Protein Data Bank file 1FE1). We note that rings I and III are B and D in file 1DOP. Since the X-ray structure[10] did not provide the orientation of the transition dipoles, we have adopted orientations which most closely resembled the dipole orientations in Svensson's computer model structure. Given that there is some uncertainty in the coordinates of both structural models, it was decided that calculation of the

TABLE 1: Excitonic Multimer Hamiltonians for the PSII RC[a]

	$Pheo_1$	Chl_1	P_2	P_1	Chl_2	$Pheo_2$
$Pheo_1$	$\epsilon + d_1$	**86.7**	**15.7**	**−2.9**	**−5.8**	**2.1**
		4.6	*−0.5*	*−3.1*	*−0.3*	*0.5*
		(87.3)	(19.5)	(−15.2)	(−6.4)	(4.6)
Chl_1		$\epsilon + d_2$	**−77.7**	**−16.3**	**17.7**	**−5.0**
			2.8	*4.0*	*−0.7*	*−0.5*
			(−84.6)	(−54.1)	(8.6)	(−5.4)
P_2			$\epsilon + d_3$	**143.2**	**−78.3**	**−5.0**
				11.3	*−2.1*	*−3.2*
				(139.3)	(−56.4)	(−13.3)
P_1				$\epsilon + d_4$	**−103.6**	**12.9**
					3.0	*−0.7*
					(−83.9)	(18.2)
Chl_2					$\epsilon + d_5$	**74.9**
						4.0
						(91.7)
$Pheo_2$						$\epsilon + d_6$

[a] Numbers in bold and in parentheses are for the Q_y Hamiltonians for models I and II, respectively; $\epsilon_n = 14859$ cm^{-1}. The numbers in italics define the Q_x Hamiltonian, model I. For the Q_x states ϵ_n values of 17241 cm^{-1} for the Chl *a* molecule and 18369 and 18477 cm^{-1} for $Pheo_1$ and $Pheo_2$ were used. The d_n values are offsets due to energy disorder (see the text).

V_{nm} using point monopoles was unwarranted. The neglect of the electron-exchange coupling contribution to V_{nm} is reasonable given that the center to center distances between chlorins are $\gtrsim$10 Å. The model I Hamiltonian for the Q_y states is defined by the numbers in bold in Table 1 and is further discussed in section 4.A. Our coupling matrix elements based on model I are slightly different from those reported in ref 43 since the V_{nm} values reported in ref 43 (also based on the PSII RC coordinates of Svensson et al.[7]) were obtained with the inverted symmetry assignment, meaning that the D_1 and D_2 branches were interchanged (data not shown). In addition, our calculations revealed slightly different orientations of the monomer Q_y transition dipoles for the P_2 and Chl_2 chromophores of the D_2 branch. Similar dipole−dipole interaction energies for the Q_y transitions were obtained on the basis of the Zouni et al. X-ray coordinates (3.8 Å resolution), and are given for comparison in parentheses in Table 1 (model II Hamiltonian).

Diagonal energy disorder was taken into account by Monte Carlo simulations with random disorder at each cofactor described by a Gaussian SDF of width 210 cm^{-1}. Spectral hole-burning studies of several photosynthetic complexes have shown that the SDFs of Q_y states are uncorrelated.[39] Thus, the SDFs of the chlorins were taken to be uncorrelated. For each realization of chlorin site energies, the Hamiltonian matrix was diagonalized to obtain the excitonic energies (E_α) and wave functions

$$|\alpha\rangle = \sum_n c_{\alpha n}|n\rangle \qquad (2)$$

Since overlap is neglected, $\sum_n |c_{\alpha n}|^2 = 1$. The excitonic transition dipoles were calculated using

$$\hat{\boldsymbol{\mu}}_\alpha = \sum_n c_{\alpha n}\hat{\mu}_n \qquad (3)$$

where $\hat{\boldsymbol{\mu}}_n$ is the transition dipole of chlorin n. The optical properties of each RC were calculated using the eigenvalues and eigenvectors. Absorbance spectra and the contributing bands from the five exciton states were obtained by an ensemble averaging with energetically sorted eigenvalues and corresponding eigenvectors. Absorbance and delta absorbance (ΔA) spectra were calculated with 5 and/or 10 cm^{-1} resolution. In the calculation of the exciton density of states, the number of states in 10 cm^{-1} intervals was counted. All results presented correspond to ensemble averaging over 5000 RCs. The spatial extent (delocalization) of the exciton states (N_{del}) was calculated using $N_{del} = 1/\sum_n |c_{\alpha n}|$,[4] where N_{del} is the number of Chl molecules that contribute to exciton state α.[40]

Excitonic calculations were also performed for the Q_x states of the six cofactors with dipole strengths of 2.3 and 1.4 D^2 for Chl *a* and Pheo *a*, 10% of the values for the Q_y states.[41] The model I excitonic couplings for Q_x states given in italics in Table 1 were used. ϵ_n values of 17241 cm^{-1} (580.0 nm) for all Chl *a* molecules, 18369 cm^{-1} (544.4 nm) for $Pheo_1$, and 18477 cm^{-1} (541.2 nm) for $Pheo_2$ were used. The SDFs were as defined above for the Q_y states and were also taken to be uncorrelated. The main objective of these calculations was to show that the excitonic couplings for the Q_x states are too weak to result in motional narrowing of the inhomogeneously broadened Q_x absorption bands due to excitonic delocalization. That is, the Q_x states are, for all intents and purposes, localized on individual chlorins.

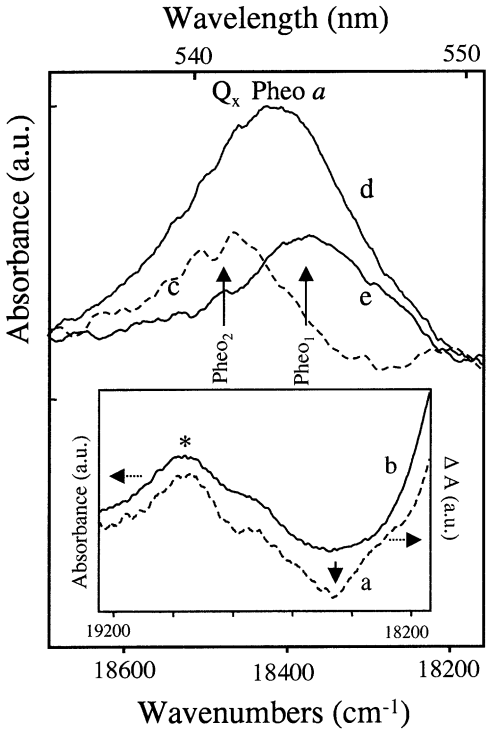

Figure 2. Pheo Q_x absorption band of RC-5 at 543 nm (d). Spectrum a is the difference between absorption after dark reduction with dithionite and absorption of untreated RC-5 from ref 22. The asterisk labels the β band of Cyt b_{559} near 530 nm. Spectrum b in the inset corresponds to the absorption spectrum of "pure" Cyt b_{559} in a protein mass from which all cofactors were extracted. Curve c is the difference between curves a and b from the inset, and corresponds to the chemically prereduced Q_x band of $Pheo_2$ at 541.2 nm. Spectrum e is the difference between spectra d and c, and corresponds to the Q_x band of $Pheo_1$ at 544.4 nm. $T = 4.2$ K.

4. Results and Discussion

A. Dark Reduction Experiments with Dithionite and Q_x Excitonic Calculations. The 4.2 K results in Figure 2 for RC-5 lead to positions and widths of the Q_x bands of $Pheo_1$ and $Pheo_2$ that are in close agreement with those reported in ref 22. Curve d is the Pheo Q_x band of an untreated (unreduced) sample. Curve b is the spectrum of a sample of protein mass containing Cyt

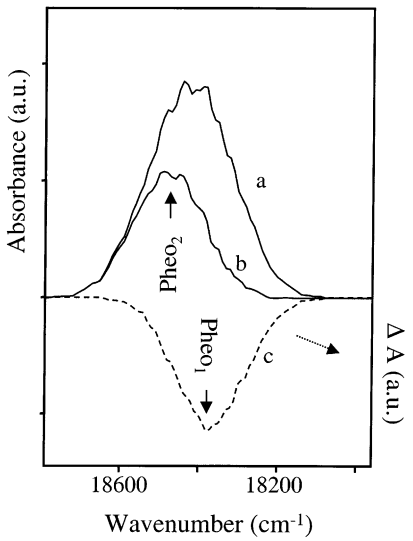

Figure 3. Spectra a and b correspond to the calculated absorption of the Pheo Q_x transition before and after deletion of the active $Pheo_1$ from the hexamer of chlorins. The b−a profile (c) is identical to the $Pheo_1$ Q_x band.

b_{559} which was reduced with dithionite. The protein mass exhibited no absorption in the Q_y region and, thus, was depleted of chlorins. The asterisk locates the β band of reduced Cyt $b_{559}^{\bullet -}$. The increase in absorption that begins near 18100 cm^{-1} is due to the α band of Cyt b_{559} with a maximum at 556.6 nm. Spectrum a is the difference between the postreduction and prereduction spectra of an RC-5 sample. As expected, the β band of Cyt b_{559} is also observed. The downward arrow in spectrum a locates the putative position of the Q_x band of $Pheo_2$. The inverted difference between spectra a and b (normalized to the same intensity at the maximum of the β band) is profile c, which is very similar to the Q_x band of $Pheo_2$ reported in ref 22. The difference between spectra d and c, profile e, is then expected to be the Q_x band of $Pheo_1$. Indeed, profile e is in close agreement with the Q_x band of $Pheo_1$ reported in ref 22.

Excitonic calculations for the Q_x states were performed using the model I multimer Hamiltonian defined in Table 1. Profile a of Figure 3 is the Q_x band contributed to by both $Pheo_1$ and $Pheo_2$ with a maximum at 543.3 nm, very close to the experimental value of 543.0 nm. Spectrum b is the result of a calculation in which $Pheo_1$ was removed from the Hamiltonian to simulate photoreduction with dithionite to $Pheo_1^-$. The position and width of profile b are 541.2 nm and ∼210 cm^{-1}. The difference between spectra b and a is profile c with a maximum at 544.4 nm and width of ∼200 cm^{-1}. That the spectral characteristics of profiles b and c are nearly identical to the experimental Q_x bands of $Pheo_2$ and $Pheo_1$ establishes that the Q_x coupling energies are too small to result in motional narrowing of the SDFs. Although the absence of appreciable narrowing due to excitonic delocalization was anticipated, given that the excitonic couplings are very small compared to the SDF widths, it was important to establish that this is the case since our arriving at the pentamer model for the Q_y states was based, in part, on consideration of experimental results on motional narrowing. The calculations showed that the two Q_x states are highly localized on $Pheo_1$ and $Pheo_2$. The above findings also emerged when $Pheo_2$ was deleted from the Hamiltonian. The localized Q_x states of the Chl molecules were hardly affected by deletion of either Pheo molecule.

B. Femtosecond Pump−Probe Spectra of the Pheo Q_x Band at 543 nm. Here we analyze the femtosecond pump−probe spectra (7 K) reported by Greenfield et al.[31] on RC-6

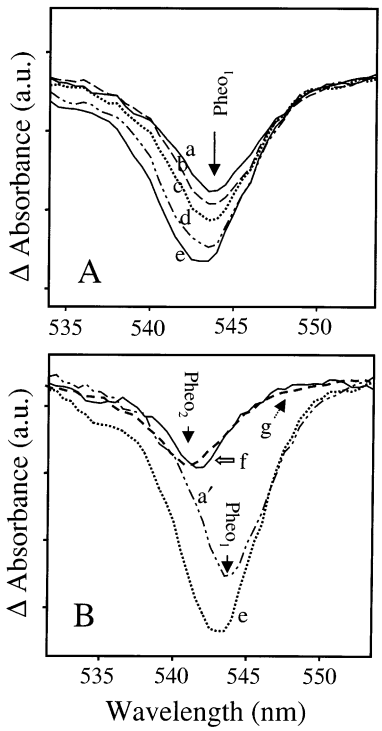

Figure 4. Frame A: Expanded transient absorption spectra in the Pheo *a* region of the isolated PSII RC-6 at 7 K from ref 31. Δ*A* spectra were recorded at different delay times, 0.5 ps (a), 1 ps (b), 10 ps (c), 100 ps (d), and 2 ns (e), after a 100 nJ, 683 nm excitation pulse. Frame B: Spectrum a′ is curve a from frame A multiplied by a factor of 1.35 to fit the low-energy side of curve e obtained with a 2 ns delay. Spectrum f (solid line) is the difference between spectra e and a′, while the dashed curve (g) corresponds to the Q_x band of $Pheo_2$ taken from ref 22 (copyright 1999 American Chemical Society).

using their original data set. The analysis provides additional support for the pentamer model in which the Q_y state of $Pheo_2$ is decoupled from those of the other core cofactors and contributes little to absorption in the vicinity of 680 nm. Greenfield et al. reported a large prompt (≲200 fs) bleach of the Pheo Q_x band upon excitation at 683 nm, a wavelength that should be quite selective for P680. They concluded that the primary charge separation rate is $(5\ ps)^{-1}$. The amplitude of the prompt bleach was about two-thirds of the final amplitude following reduction of the active $Pheo_1$. On the basis of an earlier determination of the rate for intrinsic charge separation following excitation of P680, the assignment of the prompt bleach to ultrafast primary charge separation was considered unlikely. Greenfield et al. argued that the instantaneous bleach was too strong to be due to formation of $^1Pheo_1$* by excitation of a localized $Pheo_1$ Q_y state that absorbs near P680. They favored an interpretation which is based on excitation of hexamer states that are strongly absorbing and contributed to by the Pheo molecules, although no excitonic calculations to provide support were performed.

Greenfield et al. did not attempt to determine the contributions of $Pheo_1$ and $Pheo_2$ to the bleach of the Q_x band. That this is possible is illustrated in Figure 4A, where their transient spectra obtained with 683 nm excitation are replotted for delay times of 0.5 ps (a), 1.0 ps (b), 10 ps (c), 100 ps (d), and 2 ns (e). A blue shift and broadening of the Q_x bleach with time are clearly evident, indicating that at early times (≲10 ps) the bleach is dominated by $Pheo_1$. The 0.5 ps profile is centered at 544 nm and carries a width of ∼200 cm^{-1}. The width of the 2 ns profile at 543 nm is ∼300 cm^{-1}. This profile is very similar to the Q_x

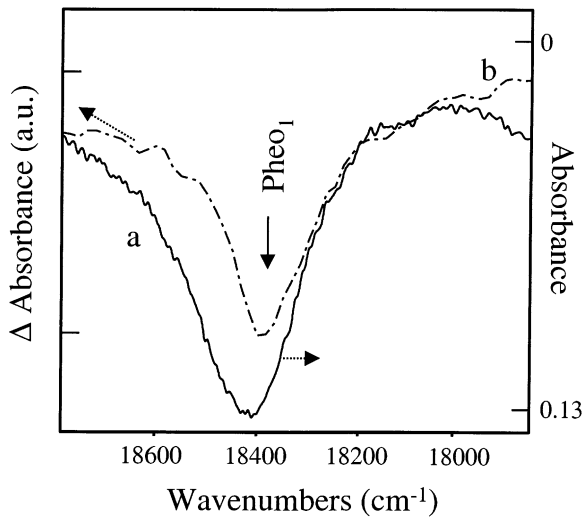

Figure 5. Spectrum a corresponds to the inverted Pheo Q_x absorption band at 4.2 K. Curve b is the difference between transient absorption spectra of the RC-6 (at 7 K) recorded at a 0.5 ps delay time, obtained for excitation wavelengths of 683 and 661 nm.

absorption band. Figure 4B provides a different view of the time evolution. Spectrum e is profile e (2 ns delay) of Figure 4A. Profile a′ is spectrum a (0.5 ps delay) of Figure 4A, but multiplied by a factor of 1.35 to fit the low-energy side of spectrum e. Spectrum f is the e−a′ difference spectrum, which should be compared with curve g, which is the $Pheo_2$ Q_x band for RC-6 reported in ref 22. The quite close agreement between spectra f and g shows that $Pheo_2$ contributes to the bleach at longer times, but relatively weakly. Presumably, the contribution from $Pheo_2$ to the bleach is due to energy equilibration between the higher energy delocalized Q_y states with the localized $Pheo_2$ Q_y state that follows relaxation of the Q_x state of $Pheo_1$. The absence of a contribution from $Pheo_2$ to the prompt bleach following excitation at 683 nm is consistent with our pentamer model.

Additional support for the above conclusions is provided by comparison of the 0.5 ps spectra obtained with red excitation at 683 nm and blue excitation at 661 nm. Importantly, the Q_x bleach obtained with the latter excitation does not change shape with increasing probe delay and is very similar to the Q_x absorption band.[31] We note that the pulses carried a width of ∼6 nm so that, with 661 nm excitation, direct population of the 668.3 nm $Pheo_2$ Q_y state (absorption bandwidth of ∼3.6 nm) should occur. Direct excitation of pentamer states contributed to by $Pheo_1$, either through origin or vibronic states, is also possible. A firm understanding of the apparent time independence of the bleach with 661 nm excitation would require determination of the energy-transfer and equilibration kinetics following excitation of states in the vicinity of 661 nm. In Figure 5, spectrum a is the inverted Q_x absorption band and spectrum b is the difference between the bleach profiles obtained with 683 and 661 nm excitation. This difference spectrum is similar to spectrum a of Figure 4A, which is the bleach (0.5 ps delay) produced with 683 nm excitation. The similarity is consistent with only $Pheo_1$ contributing to the prompt bleach observed with 683 nm excitation.

C. Q_y Excitonic Calculations with the Pentamer Model and Comparison with Experiment. As mentioned in the Introduction, an earlier study on RC-5 had shown that dark reduction with dithionite does not produce a strong bleach in the 680−684 nm region, as expected if $Pheo_2$ is excitonically coupled to the remaining RC chlorins. (Results presented above for the Q_x band established that $Pheo_2$ is reduced.) That the dominant effect of $Pheo_2$ reduction is a bleach at 668.3 nm with a width of ∼200 cm^{-1} was also confirmed during the course of our study of the Pheo Q_x band. This led us to consider that $Pheo_2$ is, for all intents and purposes, excitonically decoupled from the other five core cofactors, i.e., to the pentamer model. Further support for the decoupling came from the observation that the widths of the $Pheo_2$ Q_x and Q_y bands at 541.2 and 668.3 nm are nearly identical, ∼200 cm^{-1}, and dominated by inhomogeneous broadening. In addition, the very recent work of Germano et al.,[44] performed on RC-6 with modified Pheo *a* composition, has not shown much evidence for the involvement of $Pheo_2$ in excitonic interactions. We note that the 4.2 K widths of the Q_x and Q_y bands of a Chl *a* monomer in glasses are also similar.[37,45] Thus, it is reasonable to assume that the widths of the SDF for the Q_x and Q_y states of "monomer" $Pheo_2$ (or $Pheo_1$) in the RC are equal. (This might be expected given that the electronic parentages of the Q_x and Q_y states are the same.) However, if the Q_y state of $Pheo_2$ is involved in delocalization, one expects significant motional narrowing of the inhomogeneous broadening of an absorption band to which $Pheo_2$ contributes significantly; see below. The absence of such narrowing is consistent with the 668.3 nm state being highly localized on $Pheo_2$. The question of why is addressed at the end of section 4.C.

The resulting models I and II pentamer Hamiltonians are obtained from the two Hamiltonians in Table 1 by setting the coupling energies involving $Pheo_2$ to zero and the wavelength of the localized $Pheo_2$ state to 668.3 nm. From that table one sees that to achieve localization the $Pheo_2$−Chl_2 coupling of ∼80−90 cm^{-1} would have to be markedly reduced.

The results of the pentamer calculations that follow were obtained using the same SDF for each of the five chlorins, a Gaussian centered at 673 nm with a width of 210 cm^{-1}. Calculations of the type described below with a width of 210 cm^{-1} were also performed using considerably smaller values for the SDF width of the core Chl molecules. However, the resulting Q_y absorption and triplet bottleneck hole-burned spectra were found to exhibit features that are too sharp relative to those of the experimental spectra (results not shown). In addition, it was found that random variations of the site energies of the four core Chl molecules over a ±2.5 nm (±50 cm^{-1}) interval about 673 nm had only a small effect on the spectra, as might be expected since the 100 cm^{-1} interval is small relative to the 210 cm^{-1} width of the SDF.

Q_y Absorption Spectrum. The Q_y absorption spectrum of PSII RC calculated with the pentamer model I is shown in Figure 6A (solid line). The averaged exciton density of states is shown in the inset. The absorption spectrum calculated with the model II parameters was similar, as might be expected given the similarity of the two Hamiltonians in Table 1, though with slightly stronger absorption near 670 nm (spectrum not shown). The 670 nm band in Figure 6A is contributed to by the localized $Pheo_2$ band (dotted line). The dashed curves correspond to the five exciton states summarized in Table 2A. As illustrated in Table 2B, model II shows very similar exciton bands and occupation numbers for the five chlorins. The solid curve should be compared with the experimental absorption spectrum shown in Figure 1. Recall that the calculated spectrum does not include the contribution from the remaining Chl_Z molecule since the position of its absorption band is still a matter of debate.[17,22] Although the calculated spectrum correctly predicts that the most intense feature is near 680 nm, it underestimates the absorption intensity in the ∼670−675 nm region. This is also true for the

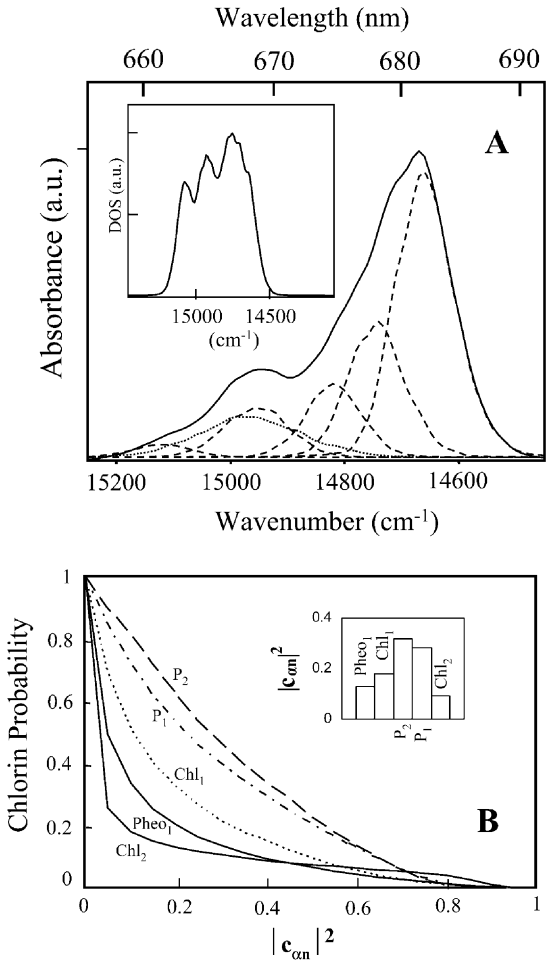

Figure 6. Frame A: RC-5 Q_y absorption spectrum (solid line) and exciton bands (dashed lines) calculated with the model I pentamer Hamiltonian. The spectrum includes the contribution from decoupled $Pheo_2$ (dotted curve). The contribution from peripheral chlorophylls is not included. The inset shows the calculated density of states generated by an ensemble average over 5000 RCs. Frame B: Probability of finding an RC as a function of the occupation number $|c_{\alpha n}|^2$ for each chlorin with $\alpha = P_1$, P_2, Chl_1, Chl_2, and $Pheo_1$. The inset shows the averaged occupation number of the contributing cofactors to the lowest energy exciton state, $Pheo_1$ (0.13), Chl_1 (0.18), P_2 (0.32), P_1 (0.28), Chl_2 (0.09).

TABLE 2: Averaged Absorption Maxima, Dipole Strengths, and Chlorin Occupation Numbers[a]

exciton band max (±0.1 nm)	dipole strength (Chl *a* monomer unit)	occupation numbers for the five chlorins				
		$Pheo_1$	Chl_1	P_2	P_1	Chl_2
A. Pentamer Model I of the PSII RC						
682.0	2.3	0.13	0.18	0.32	0.28	0.09
678.2	1.1	0.18	0.18	0.14	0.22	0.28
674.8	0.6	0.21	0.16	0.18	0.13	0.32
668.8	0.5	0.45	0.37	0.04	0.06	0.08
661.3	0.1	0.03	0.11	0.32	0.31	0.23
B. Pentamer Model II of the PSII RC						
682.0	2.23	0.15	0.19	0.32	0.26	0.08
678.2	1.12	0.16	0.22	0.14	0.26	0.22
674.9	0.50	0.21	0.14	0.17	0.10	0.38
668.8	0.67	0.44	0.26	0.06	0.06	0.18
661.1	0.08	0.04	0.19	0.31	0.31	0.15

[a] The decoupled $Pheo_2$ band is at 668.3 nm with a dipole strength of 0.61 (Chl *a* monomer unit). The widths of all absorption bands are 120 ± 10 cm^{-1}, the result of motional narrowing (see the text).

model II Hamiltonian, although in this case, as shown in Table 2B, the exciton bands near 675 and 669 nm have slightly weaker and stronger dipole strengths, respectively, than those calculated with the model I parameters and given in Table 2A. Inclusion of vibronic transitions that build on the origin transitions near 680 nm would increase absorption in the above region, but on the basis of the Chl *a* Franck−Condon factors reported in refs 46 and 47 not by an amount sufficient to bring the calculated and experimental spectra into close agreement. In the absorption spectrum of Figure 6A (solid line) the ratio of the intensity of the maximum at ~682 nm to that of the maximum near 670 nm is ~3. Inclusion of vibronic transitions decreases the ratio to only ~1.5. Random variation of the five site excitation energies as described above did not significantly enhance absorption in the 670−675 nm region. However, the spectrum shown in Figure 1 is for an RC-5 sample containing 5.2 ± 0.3 Chl molecules. Given this uncertainty, it is possible that not all of the peripheral Chl molecules absorbing near 670 nm were removed. The addition of an absorption equivalent to that of 0.5 Chl molecule at ~670 nm and a small red shift of the Q_y transition of $Pheo_2$ would result in reasonable agreement between the calculated and experimental spectra (results not shown). It is also possible that the unremoved Chl_Z may absorb near 670 nm rather than 684 nm (as assigned in ref 22).

Q_y Exciton Bands. The ensemble-averaged absorption maxima and intensities of the Q_y exciton states calculated with the models I and II pentamer Hamiltonians are given in Table 2. (We emphasize that the results given in Table 2A and shown in Figures 6−9 were obtained by energetically ordering the exciton states for the entire ensemble of RCs.) The state localized on $Pheo_2$ at 668.3 nm (fwhm ≈ 210 cm^{-1}) is included in the absorption spectrum shown in Figure 6A but is not listed in Table 2. The other five states exhibit delocalization over $N_{del} \approx 2.7$ chlorins, consistent with their similar (~120 ± 10 cm^{-1}) calculated bandwidths. Excitonic delocalization should narrow the 210 cm^{-1} inhomogeneous broadening by a factor of $\sqrt{N_{del}} \approx 1.7$ to 130 cm^{-1}, in good agreement with the calculated widths.

The delocalization patterns obtained with the Hamiltonians shown in Table 1 are not restricted mainly to the D_1 or D_2 sides, contrary to the conclusion reached by Merry et al.,[21] who used a model of the PSII RC based on the *Rps. viridis* structure.[19] Indeed, they showed that with their Hamiltonian[19] there was a tendency to localize on either the D_1 or the D_2 branch. Such a restriction is not expected in our case given that the coupling between P_1 and P_2 is significantly stronger than the other pairwise interactions. In view of this we performed calculations with the models I and II multimer Hamiltonians given in Table 1. It was found that on average the six Q_y states are delocalized over both branches.

The averaged compositions of the five exciton states are given in Table 2. For example, the lowest energy state at 682.0 nm in model I is delocalized over $Pheo_1$ (13%), Chl_1 (18%), P_2 (32%), P_1 (28%), and Chl_2 (9%). Similar delocalization is observed with the model II parameters (see Table 2B). For ease of inspection, the occupation numbers of the chlorins contributing to the 682.0 nm state are shown for model I in the inset of Figure 6B. Note that this state carries an average dipole strength of 2.3 Chl *a* monomers and ~40% of the total absorption intensity. The dipole strength of the second lowest state at 678.2 nm is equivalent to that of ~1.1 Chl *a* monomers.

Taking into account the contributions from $Pheo_1$ to the 682.0 and 678.2 nm states given in Table 2A and that the dipole strength of monomer Pheo is ~60% that of monomer Chl, it follows that the combined dipole strength of $Pheo_1$ for the two states is equivalent to that of 1.8 Pheo monomers. As mentioned,

Greenfield et al.[31] observed a large prompt bleach ($T = 7$ K) of the Pheo Q_x band upon excitation at 683 nm with femtosecond pulses carrying a width of 6 nm that could not be understood in terms of excitation of a single Pheo monomer. A similar prompt bleach ($T = 10$ °C) of the Pheo Q_x band was also observed by Merry et al.[21] (We have assigned the prompt bleach mostly to $Pheo_1$, vide supra.) We propose that the 6 nm wide pulses in ref 31 excited both of the above states with a combined $Pheo_1$ dipole strength equivalent to that of about two $Pheo_1$ monomers and that this is responsible for the large prompt bleach of the $Pheo_1$ Q_x band. The state of affairs is that excitonic mixing of the $Pheo_1$ Q_y state with the Chl *a* Q_y states leads to it "borrowing" intensity from the more strongly absorbing Chl *a* molecules. Figure 6B provides further insight into the chlorins that contribute to the lowest energy and primary electron donor state. The five curves (for model I) represent the probability of finding an RC with an occupation number $|c_{\alpha n}|^2$ ($\alpha = P_1$, P_2, Chl_1, Chl_2, $Pheo_1$) that ranges from 0 to 1. The results reveal, for example, that the probabilities of finding an RC with an occupation number >0.2 on P_1, P_2, Chl_1, Chl_2, and $Pheo_1$ are ~0.6, 0.6, 0.3, 0.1, and 0.2, respectively. As another example, the probabilities for finding a highly localized state with an occupation number >0.70 on P_1, P_2, Chl_1, Chl_2, and $Pheo_1$ are about 0.07, 0.07, 0.03, 0.07, and 0.03, respectively. The results are consistent with those in the inset of Figure 6B which show that, on average, P_1 and P_2 are the most significant contributors to the primary donor state, although the contributions from Chl_1, Chl_2, and $Pheo_1$ are by no means negligible. We hasten to add that similar results were obtained with the model II Hamiltonian (results not shown). It would be interesting to determine the primary electron donor rates for single RC complexes since the distribution of rates observed, together with excitonic calculations, should shed light on which chlorins are most important for charge separation. In this regard, we note that the photon echo data ($T = 1.33$ K) of Prokorenko and Holtzwarth[43] on bulk RC-6 samples indicate the primary charge separation kinetics are dispersive, as might be expected in view of the results presented here.

Triplet Bottleneck Hole Spectra. To further test the pentamer model, simulations of the experimental triplet bottleneck hole-burned spectrum of RC-5 (curve a in Figure 7) were performed. As noted in the Introduction, ADMR experiments had indicated that the triplet is localized on a single Chl *a* molecule, most likely on one of the accessory Chl molecules. Therefore, calculations were performed with one of each of the chlorins P_1, P_2, Chl_1, and Chl_2 deleted. Both the models I and II pentamer Hamiltonians were used. The triplet bottleneck spectrum is the difference between the absorbance spectra with and without deletion of a chlorin. The results obtained with models I and II were quite similar. However, the best fit (curve b) to the experimental spectrum (a in Figure 7A) was obtained with deletion of Chl_1, and the model I Hamiltonian. Model II revealed a slightly deeper hole near 670 nm (data not shown) in agreement with the results given in Table 2B. The fits obtained by deletion of the Chl_2 or P_1 molecules were poor. However, acceptable fits were obtained by the deletion of P_2, the chlorin that is closest to Chl_1, especially when the parameters of model II were used. This is illustrated in Figure 7B, where spectra c and d are the experimental and calculated transient holes, respectively. The calculated spectra in Figure 7 have been shifted to the blue by 40 cm^{-1}. This shifting is of no concern since electron−phonon coupling is not accounted for in the calculations. This coupling would lead to a blue shift of ~30 cm^{-1}.[34] Shifting of the site excitation energies from 673 to 672.5 nm would result in an additional blue shift of ~10 cm^{-1}. The fit obtained by deletion of Chl_1 is quite satisfactory. Note that in Figure 7 even the weak feature at 667 nm is reproduced. Detailed analysis revealed that the 667 nm hole is mainly due to the absence of the 668.8 nm exciton band (see Table 2A) to which Chl_1 contributes significantly (37%). The hole is interfered with by the absorption of the transiently decoupled $Pheo_1$ at ~673 nm. (Decoupling leads to the state at 673 nm being highly localized on $Pheo_1$, on average ~70%.)

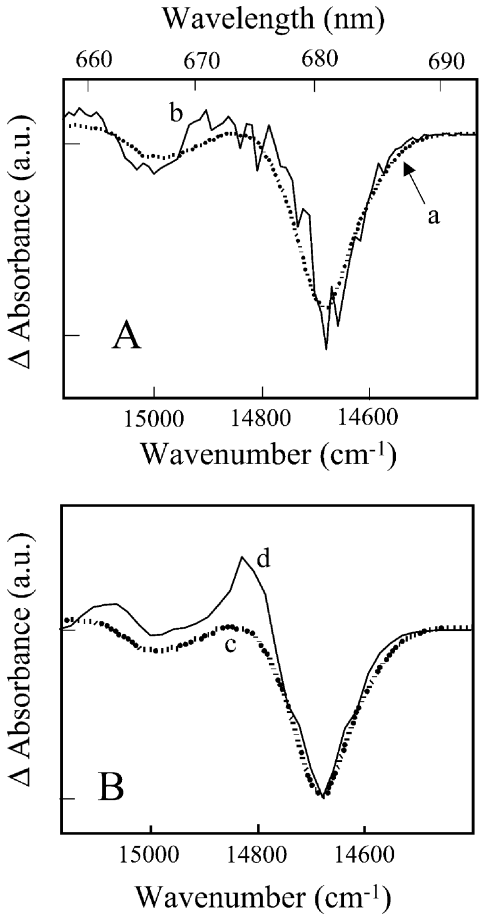

Figure 7. Frame A: Triplet bottleneck hole-burned spectrum (a) obtained at 4.2 K with $\lambda_B = 665$ nm and a burn intensity of 75 mW/cm^2 for RC-5. Spectrum b is the ΔA calculated with pentamer model I (5 cm^{-1} resolution) with Chl_1 deleted due to formation of $^3Chl_1$. Spectrum b has been shifted to the blue by 40 cm^{-1}. Frame B: Spectrum c is the same as curve a in frame A; spectrum d corresponds to the ΔA spectrum calculated with pentamer model II (10 cm^{-1} resolution) with P_2 deleted due to formation of $^3P_2$. Spectrum d has been shifted to the blue by 40 cm^{-1} (see the text for details).

Given that our results indicate that the triplet is mainly localized on Chl_1 (or P_2), we calculated the Q_y absorption spectrum with Chl_1 (or P_2) deleted from the model I pentamer Hamiltonian. The calculation neglects the difference between $^3Chl_1$ and $^1Chl_1$ on the dispersion interactions that affect the energies of the Q_y states. However, this difference should mainly affect the energies rather than the spectral features of the Q_y absorption spectrum. The result of Chl_1 deletion is shown in Figure 8A (solid curve). The dashed curves are the contributions from the four Q_y exciton states, with the asterisk locating the state mainly localized on the decoupled $Pheo_1$. (The dotted curve is the absorption due to the decoupled $Pheo_2$.) The band maxima, widths, absorption intensities, and contributions from P_1, P_2, $Pheo_1$, and Chl_2 to those states are given in Table 3A. Comparison of this table with Table 2A is instructive. For

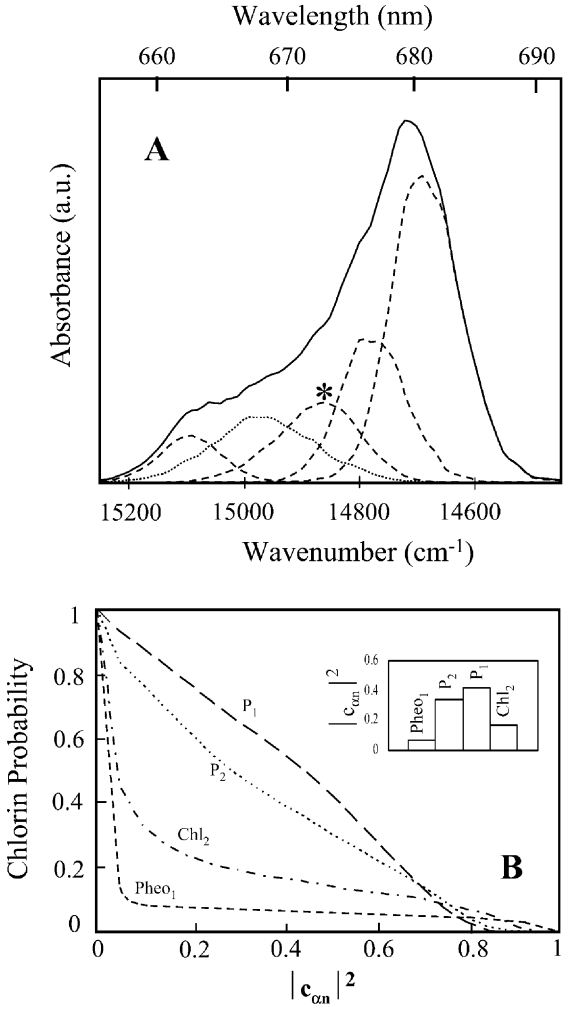

Figure 8. Frame A: RC-5 Q_y absorption spectrum (solid line) and four exciton bands (dashed lines) calculated with the pentamer model I Hamiltonian with Chl_1 deleted due to formation of $^3Chl_1$. The absorption spectrum includes the contribution from decoupled $Pheo_2$ (dotted line). The band labeled with an asterisk mainly corresponds to the decoupled $Pheo_1$. Frame B: Probability of finding an RC as a function of the occupation number $|c_{\alpha n}|^2$ for each chlorin with $\alpha = P_1$, P_2, Chl_2, and $Pheo_1$. The inset shows the averaged occupation number of the contributing cofactors to the lowest energy exciton state, $Pheo_1$ (0.07), P_2 (0.34), P_1 (0.42), and Chl_2 (0.17).

example, the bandwidths for all five states in Table 2A are motionally narrowed from the SDF width of 210 cm^{-1} to ~120 cm^{-1} due to excitonic delocalization. Only the absorption bands at 681.0, 676.8, and 662.8 nm in Table 3 are motionally narrowed to ~120 cm^{-1}. The 673.0 nm band is only slightly narrowed to 180 cm^{-1} because it stems from a state that is highly localized on $Pheo_1$ due to its transient decoupling from Chl_1.

As another example, deletion of Chl_1 from the excitonic system blue shifts the lowest energy state to 681.0 nm and significantly increases the contributions from P_1 and P_2 to it, Table 3A and inset of Figure 8B. Their average occupation numbers are 0.42 and 0.34. The four curves in Figure 8B represent the probability of finding an RC with an occupation number $|c_{\alpha n}|^2$ ($\alpha = P_1$, P_2, Chl_2, $Pheo_1$) that ranges from 0 to 1. Comparison of the P_1 and P_2 curves with those of P_1 and P_2 in Figure 6B reveals in a different way that deletion of Chl_1 leads to increased P_1 and P_2 participation in the lowest energy Q_y state. The probabilities of finding an RC with an occupation number >0.2 for P_1 and P_2 are now 0.74 and 0.6, respectively.

TABLE 3: Averaged Absorption Maxima, Dipole Strengths, and Chlorin Occupation Numbers

A. Pentamer Model I of the PSII RC with Chl_1 Deleted Due to Formation of $^3Chl_1$

exciton band max (±0.1 nm)	dipole strength (Chl *a* monomer unit)	occupation numbers for the four chlorins			
		$Pheo_1$	P_2	P_1	Chl_2
681.0	1.90	0.07	0.34	0.42	0.17
676.8	0.85	0.23	0.23	0.14	0.40
673.0	0.60	0.69	0.09	0.06	0.16
662.8	0.25	0.01	0.34	0.38	0.27

B. Pentamer Model II of the PSII RC with P_2 Deleted Due to Formation of $^3P_2$

exciton band max (±0.1 nm)	dipole strength (Chl *a* monomer unit)	occupation numbers for the four chlorins			
		$Pheo_1$	Chl_1	P_1	Chl_2
679.8	1.08	0.23	0.29	0.27	0.21
676.4	1.52	0.26	0.23	0.24	0.27
670.3	0.55	0.28	0.20	0.20	0.32
665.9	0.45	0.22	0.29	0.29	0.20

Deletion of P_2 from the excitonic system blue shifts the lowest energy state to 679.8 nm and significantly decreases and increases the dipole strength of the first and second lowest exciton bands, respectively. The averaged absorption maxima, dipole strengths, and chlorin occupation numbers for the model II pentamer model of the PSII RC with P_2 deleted due to formation of $^3P_2$ are summarized in Table 3B. The values of the dipole strengths and chlorin occupation numbers of the two lowest exciton bands in Table 3B explain why the calculated ΔA values shown in Figure 7B (curve d) with P_2 deleted due to formation of $^3P_2$ are strongly positive near 676 nm. Therefore, we conclude that formation of either $^3(P_2)$ or $^3(Chl_1)$ can explain the triplet bottleneck spectra.

Photoreduction of $Pheo_1$. As mentioned in the Introduction, the active $Pheo_1$ can be reduced by dithionite plus white light illumination.[23−25] The result of such an experiment on RC-5 at 4.2 K[22] is spectrum a in Figure 9. The main point is that since $Pheo_1$ contributes to the strongly absorbing, lowest energy Q_y state (Tables 2A and 2B), one would expect a prominent bleach near 680 nm, as observed. The bleach at 680.6 nm corresponds to a 0.1 fractional absorbance change. The bleaching profile due to formation of $Pheo_1^-$ is similar to the profile of the P680 transient hole shown in Figure 7A (spectrum a). However, in contrast with the P680 transient hole, the 680.6 nm band in spectrum a of Figure 9 is accompanied by a weak bleaching near 544.4 nm (not shown) that is characteristic of the Q_x band of $Pheo_1$ and has a larger absorbance increase near 673 nm and a small increase near 685−686 nm indicated by an asterisk. We have suggested previously that the latter is most likely due to red shifting of the 684 nm band.[22] In addition, the high-energy side of the main bleach in spectrum a of Figure 9 is steeper than the bleach observed in the transient P680 hole, which also suggests that the electrochromic shift cannot be neglected. The positive ΔA near 673 nm in spectrum a of Figure 9 is also consistent with the pentamer model since photoreduction of $Pheo_1$ does not lead to the formation of the 673 nm band due to decoupled $Pheo_1$. To simulate the $Pheo_1^-$ ΔA spectrum, one needs to take into account the electrochromic shift since white light reduction of $Pheo_1$ accumulates Cyt b_{559}^+ P680 $Pheo_1^-$, leading to a shift of the absorption spectrum. Thus, the $Pheo_1^-$ ΔA spectrum was calculated as the difference between the pentamer absorption and the absorption of the pentamer with $Pheo_1$ deleted from the model I Hamiltonian, with the latter

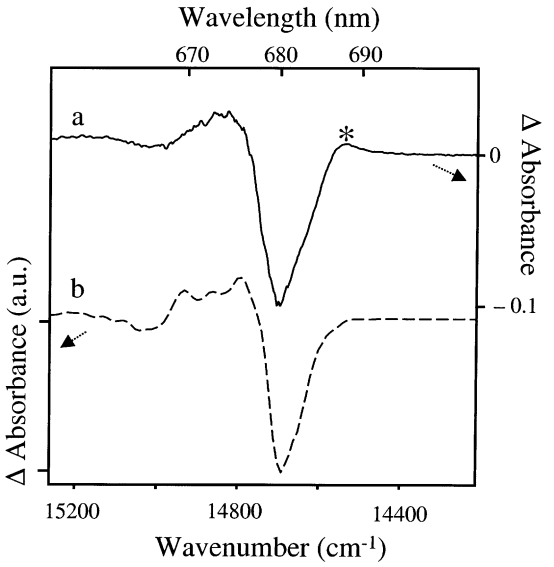

Figure 9. Spectra a and b correspond to the bleaching spectrum due to formation of $Pheo_1^-$ and the calculated ΔA spectrum simulating reduction of $Pheo_1$ ($Pheo_1^-$), respectively. The experimental ΔA spectrum was obtained following illumination at 4.2 K of RC-5 in the presence of dithionite; spectrum b was obtained by deleting $Pheo_1$ from the pentamer model I excitonic Hamiltonian. The calculated spectrum includes the electrochromic shift (see the text).

spectrum blue-shifted to account for the anticipated electrochromic shift. Both Hamiltonians provided similar spectra; however, the best fit to spectrum a was obtained with the model I parameters and a 25 cm^{-1} blue electrochromic shift. The calculated spectrum b was further blue-shifted (40 cm^{-1}) to account for the shift due to electron−phonon coupling (vide supra). Since curves a and b are very similar, we conclude that photoreduction of $Pheo_1$ is also consistent with the pentamer model.

Decoupling of $Pheo_2$ from the Q_y Excitonic System. The experimental results presented here and in ref 22 strongly indicate that while $Pheo_1$ plays an important role in delocalization of the core Q_y states, $Pheo_2$ does not. The models I and II pentamer Hamiltonians provide a good description of the frequency and time domain spectra. The key question is why $Pheo_2$ is decoupled. On the basis of the hexamer Hamiltonians in Table 1, it is clear that decoupling would require a large reduction (∼10×) of the ∼80−90 cm^{-1} $Pheo_2$−Chl_2 coupling. Unfortunately, the 3.8 Å resolution structure is too low to shed light on how such a reduction might arise. Besides, the dipole moment orientation of $Pheo_2$ was selected in a way that it was similar to that given in the Svensson et al. model structure. Modeling studies, however, suggest that the H-bonding of $Pheo_1$ and $Pheo_2$ is different;[48] specifically, while both have a H-bond to the keto group on ring V, only $Pheo_1$ appears to have a H-bond to the ester oxygen on the phytol branch. But it is not clear why such a difference would lead to decoupling. Interestingly, we found that in-plane rotation of the Q_y transition dipole (parallel to the N_I−H···N_{III}−H axis) by 90° reduces the $Pheo_2$−Chl_2 coupling by a factor of 12, which is large enough to effectively decouple $Pheo_2$. The rotation would not need to be so large provided the local dielectric screening of the $Pheo_2$−Chl_2 interaction was correspondingly large. As to why such a rotation might occur, we can only speculate at this time. One possibility is that $Pheo_2$ is in an environment that is acidic enough to lead to its protonation at the nitrogen of ring II. Lötjönen and Hynninen[48] have shown that formation of the monocation results in significant redistribution of electron density in the ground state, which might lead to reorientation of the transition dipole. Another possibility is that the stacking forces produce a distortion of the $Pheo_2$ macrocycle that is large enough to result in the tautomer with the N−H bonds at rings II and IV lying lowest in energy.[49] A high-resolution X-ray structure of the PSII RC would allow for testing of these speculative ideas.

5. Concluding Remarks

Experimental results presented here and in refs 22 and 31, together with excitonic calculations, have led us to propose a pentamer model for the core Q_y states of the PSII RC in which $Pheo_2$ is essentially decoupled from the other five chlorins. For both the models I and II pentamer Hamiltonians, four of the five states are delocalized over both the D_1 and D_2 branches, Table 2. Delocalization over both branches was also found for the Q_y states of the models I and II *multimer* Hamiltonians defined in Table 1. This is in contrast with the conclusion reached in ref 21, based on the Hamiltonian reported in ref 19, that delocalization is mainly restricted to either the D_1 or D_2 branch. Although the tendency to localize either on D_1 or D_2 has been observed[21] with the original (*Rps. viridis* based) Hamiltonian for the PSII RC reported in ref 19, the localization/delocalization patterns are significantly different when calculated with the Hamiltonians given in Table 1. That is, with the V_{nm} values given in Table 1, the lowest exciton state is localized on P_1 and P_2 in about 50% of single RCs. Finally, delocalization leads to significant motional narrowing of the inhomogeneous broadening of the Q_y absorption bands, from the 210 cm^{-1} width of the SDFs to ∼120 cm^{-1}.

Given that the Q_y states exhibit significant delocalization, the question as to the nature of the primary electron donor (PED) state P680* naturally arises. This state is expected to be the lowest energy state. The results in Table 2A for this state at 682.0 nm show that, on average, P_1 and P_2 with occupation numbers of 0.28 and 0.32 (or 0.26 and 0.32 for model II, Table 2B) make the largest contributions although those from Chl_1, $Pheo_1$, and Chl_2 are significant. The large dipole strength of 2.3 is, to a considerable extent, due to the coefficients of P_1 and P_2 in the P680* wave function carrying opposite signs, as is the case for the P_- special pair state of the bacterial RC. (The P_1 and P_2 transition dipoles are roughly antiparallel.) The "counterpart" of the 682.0 nm state is the weakly absorbing, highest energy state at 661.3 nm. In its wave function the coefficients of P_1 and P_2 tend to carry the same sign, which leads to destructive interference of their transition dipoles.

The results in Figure 6B, where the chlorin probabilities for P680* are plotted versus occupation number, are consistent with those in Table 2A but more telling in that they indicate that the chlorin composition of P680* should vary quite significantly from complex to complex. (This is due to the delicate interplay between the width of the uncorrelated SDFs and the excitonic couplings.) For example, for five randomly selected complexes it was found that the excitation is mainly confined to two chlorins: Chl_1/P_2 (63%/24%), P_1/Chl_1 (35%/51%), P_1/Chl_1 (43%/35%), P_1/P_2 (14%/75%), and P_1/P_2 (47%/47%). Thus, what P680* is depends on the complex. Moreover, it appears that the mechanism of primary charge separation and, therefore, its kinetics can vary from complex to complex. This suggests that the kinetics of a bulk sample could be dispersive, consistent with the low-temperature photon echo data in ref 43. The two P_1/P_2 single complexes are interesting in that they present a situation that is analogous to that found in the bacterial RC, where the PED state is highly localized on P_L and P_M, the special

pair. With $P_1/P_2 \equiv P$, the charge-separated state $P^+Chl_1^-Pheo_1$ would be expected to play a key role in formation of $P^+Chl_1Pheo_1^-$, either as a real intermediate state or as a virtual state (superexchange mechanism). Charge recombination within $P^+Chl_1Pheo_1^-$ would lead to triplet-state formation. The other three single complexes are also interesting. For example, the Chl_1/P_2 (63%/24%) complex is one in which Chl_1 might be targeted as the primary electron donor. The following scheme might apply: $[P_2/Chl_1]^*Pheo_1 \rightarrow [P_2/Chl_1^+]Pheo_1^- \rightarrow [P_2^+/Chl_1-Pheo_1^-]$, similar to one suggested by Prokorenko and Holtzwarth.[43] On the other hand, if P_2 is more easily oxidized than Chl_1, then P_2 would be the primary donor with a rate proportional to its occupation number.[50] Charge separation schemes such as these ignore, of course, the possibility of self-trapping at a specific chlorin due to exciton−phonon coupling, which becomes important when it is rapid relative to charge separation. At present the rate of charge separation is subject to debate with reported values ranging between (0.5 ps) $^{-1}$ and (20 ps) $^{-1}$, as reviewed in ref 50. It should be noted that the dynamics of charge separation at biological temperatures may be different from that in the low-temperature limit. At biological temperatures equilibration between the Q_y states due to exciton−phonon scattering might be rapid relative to charge separation. Moreover, Q_y states lying higher than the lowest energy state are thermally populated and might also serve as primary donor states. Clearly, understanding primary charge separation and its dependence on temperature is far more difficult than in the bacterial RC. For significant progress to be made, a high-resolution X-ray structure of the PSII RC is required so that all relevant electronic coupling matrix elements, including those involved in formation of charge-transfer states, can be accurately calculated. With the static lattice wave functions and energies in hand, it will be important to determine the charge separation dynamics in individual complexes, especially in the low-temperature limit since the Q_y absorption spectrum is more structured and better understood than at room temperature.

Finally, we comment on our finding and those of others[32,33,51] that the triplet state formed by charge recombination in $P680^+Pheo_1^-$ is most likely localized on Chl_1. Although this is consistent with Chl_1 being the primary donor, the observation of $^3Chl_1$ does not prove that this is the case. Given that the nature of P680* varies significantly from complex to complex, one can expect that different triplets are formed, e.g., $^3P_2$ and/or $^3Chl_1$. In fact, the calculated transient hole-burned spectra with Chl_1 or P_2 deleted (due to formation of $^3Chl_1$ and $^3P_2$) both provide satisfactory agreement with the experimental triplet bottleneck hole burned spectra. However, if $^3Chl_1$ lies lowest in energy, it could be populated by triplet energy transfer from $^3P_2$. Evidence for this has recently been reported by Noguchi et al.[51]

Acknowledgment. Research at the Ames Laboratory was supported by the Division of Chemical Sciences, Office of Energy Sciences, U.S. Department of Energy. Ames Laboratory is operated for the USDOE by Iowa State University under Contract W-7405-Eng-82. We thank Dr. M. Seibert and Dr. R. Picorel of the National Renewable Energy Laboratory for generously providing us with the RC preparations, Dr. M. Rätsep for experimental help during the early phase of this project, Dr. V. Zazubovich for useful discussions, Drs. S. Greenfield and M. Wasielewski for the original data files from transient absorption experiments shown in Figures 4 and 5, and Drs. W. W. Parson and H. Scheer for providing references on the Q_y transition dipole of pheophytin.

References and Notes

(1) Nanba, O.; Satoh, K. *Proc. Natl. Acad. Sci. U.S.A.* **1987**, *84*, 109.
(2) Deisenhofer, J.; Epp, O.; Miki, K.; Huber, R.; Michel, H. *J. Mol. Biol.* **1984**, *180*, 385.
(3) Trebst, A. *Z. Naturforsch.* **1985**, *41*, 240.
(4) Sayre, R. T.; Andersson, B.; Bogorad, L. *Cell* **1986**, *47*, 601.
(5) Ruffle, S. V.; Donnelly, D.; Blundell, T. L.; Nugent, J. H. A. *Photosynth. Res.* **1992**, *34*, 287.
(6) Seibert, M. In *The Photosynthetic Reaction Center*; Deisenhofer, J., Norris, J., Eds.; Academic Press: San Diego, 1993; Vol. I, p 319.
(7) Svensson, B.; Etchebest, C.; Tuffery, P.; van Kan, P.; Smith, J.; Styring, S. *Biochemistry* **1996**, *35*, 14486.
(8) Xiong, J.; Subramanian, S.; Govindjee. *Photosynth. Res.* **1998**, *56*, 229.
(9) Eijckelhoff, C.; Dekker: J. P. *Biochim. Biophys. Acta* **1995**, *1231*, 21.
(10) Zouni, A.; Witt, H. T.; Kern, J.; Fromme, P.; Krauss, N.; Saenger, W.; Orth, P. *Nature* **2001**, *409*, 739.
(11) Reddy, N. R. S.; Kolaczkowski, S. V.; Small, G. J. *J. Phys. Chem.* **1993**, *97*, 6934.
(12) Reddy, N. R. S.; Kolaczkowski, S. V.; Small, G. J. *Science* **1993**, *260*, 68.
(13) Small, G. J. *Chem. Phys.* **1995**, *197*, 239.
(14) Lyle, P. A.; Kolaczkowski, S. V.; Small, G. J. *J. Phys. Chem.* **1993**, *97*, 6926.
(15) Chang, C.-H.; Jankowiak, R.; Reddy, N. R. S.; Small, G. J. *Chem. Phys.* **1995**, *197*, 307.
(16) Wu, H.-M.; Rätsep, M.; Jankowiak, R.; Cogdell, R. J.; Small G. J. *J. Phys. Chem. B* **1998**, *102*, 4023.
(17) Kwa, S. L. S.; Eijckelhoff, E.; van Grondelle, R.; Dekker, J. P. *J. Phys. Chem.* **1994**, *98*, 7702.
(18) Chang, H.-C.; Jankowiak, R.; Yocum, C. F.; Picorel, R.; Alfonso, M.; Seibert, M.; Small, G. J. *J. Phys. Chem.* **1994**, *98*, 7717.
(19) Durrant, J. R.; Klug, D. R.; Kwa, S. L. S.; van Grondelle, R.; Porter, G.; Dekker, J. P. *Proc. Natl. Acad. Sci. U.S.A.* **1995**, *92*, 4798.
(20) Leegwater, J. A.; Durrant, J. R.; Klug, D. R. *J. Phys. Chem.* **1997**, *101*, 1, 7205.
(21) Merry, S. A.; Kamazaki, S.; Tachibana, Y.; Joseph, D. M.; Porter, G.; Yoshohara, K.; Barber, J.; Durrant, J. R.; Klug, D. R. *J. Phys. Chem.* **1996**, *100*, 10469.
(22) Jankowiak, R.; Rätsep, M.; Picorel, R.; Seibert, M.; Small, G. J. *J. Phys. Chem. B* **1999**, *103*, 9759.
(23) Tetenkin, V. L.; Gulyaev, B. A.; Seibert, M.; Rubin, A. B. *FEBS Lett.* **1989**, *250*, 459.
(24) Tang, D.; Jankowiak, R.; Seibert, M.; Yocum, C. F.; Small, G. J. *J. Phys. Chem.* **1990**, *94*, 6519.
(25) Breton, J. In *Perspectives in Photosynthesis*; Jortner, J., Pullman, B., Eds.; Kluwer Academic Publishers: Dordrecht, The Netherlands, 1989; pp 23−38.
(26) Chang, H.-C.; Small, G. J.; Jankowiak, R. *Chem. Phys.* **1995**, *194*, 323.
(27) Klug, D. R.; Rech, Th.; Joseph, D. M.; Barber, J.; Durrant, J. R.; Porter, G. *Chem. Phys.* **1995**, *194*, 433.
(28) Dìdic, R.; Lovèinsky, M.; Vácha, F.; Hala, J. *J. Lumin.* **2000**, *809*, 87.
(29) Kirmaier, Ch.; Holten, D. In *The Photosynthetic Reaction Center*; Deisenhofer, J., Norris, J. R., Eds.; Academic Press: New York, 1993; Vol. II, Chapter 3, pp 49−70.
(30) Roberts, J. A.; Holten, D.; Kirchmaier, Ch. *J. Phys. Chem. B* **2001**, *105*, 5575.
(31) Greenfield, S. R.; Seibert, M.; Wasielewski, M. R. *J. Phys. Chem. B* **1999**, *103*, 8364.
(32) van der Vos, R.; van Leeuwen, P. J.; Braun, P.; Hoff, A. J. *Biochim. Biophys. Acta* **1992**, *1140*, 184.
(33) Rutherford, A. W. *Biochem. Soc. Trans.* **1988**, *14*, 15.
(34) Zazubovich, V.; Jankowiak, R.; Rätsep, M.; Hayes, J. M.; Picorel, R.; Seibert, M.; Small, G. J. *J. Phys. Chem.*, submitted for publication.
(35) Vacha, F.; Joseph, D. M.; Durrant, J. R.; Telfer, A.; Klug, D. R.; Porter, G.; Barber, J. *Proc. Natl. Acad. Sci. U.S.A.* **1995**, *92*, 2929.
(36) Berthold, D. A.; Babcock, G. T.; Yocum, C. F. *FEBS Lett.* **1981**, *134*, 231.
(37) Eijckelhoff, C.; Dekker: J. P. *Photosynth. Res.* **1997**, *52*, 69.
(38) Svensson, B.; van Kan, P. J. M.; Styring, S. In *Photosynthesis: From Light to Biosphere*; Mathis, P., Ed.; Kluwer Academinc Publishers: Dordrecht, The Netherlands, 1995; p 425.
(39) Matsusaki, S.; Zazubovich, V., Rätsep, M.; Hayes, J. M.; Small, G. J. *J. Phys. Chem. B* **2000**, *104*, 9564 and references therein.
(40) Fidder, H.; Knoester, J.; Wiersma, D. A. *J. Chem. Phys.* **1991**, *95*, 7880.
(41) Jordanides, X. J.; Scholes, G. D.; Fleming, G. R. *J. Phys. Chem. B* **2001**, *105*, 1652.

(42) Van Amerongen, H.; Valkunas, L.; van Grondelle, R. *Photosynthetic Excitons*; World Scientific: Singapore, 2000; Chapter 7.
(43) Prokhorenko, V. I.; Holzwarth, A. R. *J. Phys. Chem. B* **2000**, *104*, 11563.
(44) Germano, M.; Shkuropatov, A. Yu.; Permentier, H.; de Wijn, R.; Hoff, A. J.; Shuvalov, V. A.; van Gorkom, H. J. *Biochemistry* **2001**, *40*, 11472.
(45) Roberts, K.; Jankowiak, R. Unpublished results.
(46) Piper, J.; Voigt, J.; Small, G. J. *J. Phys. Chem. B* **1999**, *103*, 2319.
(47) Zazubovich, V.; Tibe, I.; Small, G. J. *J. Phys. Chem. B* **2001**, *105*, 12410.
(48) Lötjönen, S.; Hymminem, P. H. *Org. Magn. Reson.* **1984**, *22*, 510.
(49) Helaya, J.; Stapelbroek-Möllman, M.; Kilpeläinem, I.; Hymminem, P. H. *J. Org. Chem.* **2000**, *65*, 3700.
(50) Dekker, J. P.; van Grondelle, R. *Photosynth. Res.* **2000**, *63*, 195.
(51) Noguchi, T.; Tomo, T.; Kato, Ch. *Biochemistry* **2001**, *40*, 2176.